Journal of *Marine Science and Engineering*

MDPI

Article

Distribution Characteristics and Evolution Mechanism of Pockmark Group in the Northwestern Xisha Uplift, South China Sea

Tianqi Lu [1,2], Yanfu Yao [1,2], Lushan Wu [1,2], Xuelin Li [1,2,*], Lei Huang [1,2] and Xuanyu Bai [1,2]

[1] Sanya Institute of South China Sea Geology, Guangzhou Marine Geological Survey, 2 Yumin Road, Sanya 572025, China
[2] Guangzhou Marine Geological Survey, China Geological Survey, 1133 Haibin Road, Guangzhou 510075, China
* Correspondence: lxlingeo@126.com; Tel.: +86-0898-88033822

Abstract

Submarine pockmarks are typical seafloor micro-geomorphic landforms formed by deep fluid seepage and sediment erosional processes. Based on high-resolution multibeam bathymetric data, multi-channel seismic sections and sediment core data, the present study systematically investigates 64 pockmarks in the northwestern Xisha Uplift, focusing on their distribution, morphology and genetic mechanisms. These pockmarks exhibit a NE–SW zonal distribution, concentrated in the 1200–1600 m central slope transition zone, and are classified into circular–elliptical, crescentic and elongated types with distinct morphometric variability. Vertically, the T40 unconformity defines the stratified geological architecture: underlying carbonate uplifts and karst-fracture systems act as fluid reservoirs and migration conduits, while overlying Late Miocene–Quaternary fine-grained hemipelagic sediments form a low-permeability caprock. Fluid overpressure accumulation and hydraulic fracturing of the caprock trigger initial pockmark formation, while spatial heterogeneity of surficial sediments and bottom-current reworking control morphological differentiation. The present study clarifies the coupled controls of deep tectono-fluid activities and shallow sedimentary and hydrodynamic processes on pockmark evolution, establishing a refined dynamic model to address the research gap regarding pockmark group genesis in the study area.

Keywords: northwestern Xisha Uplift; pockmark group; distribution characteristics; fluid activity; evolutionary mechanism

Check for updates

Academic Editor: Gemma Aiello

Received: 9 June 2026
Revised: 2 July 2026
Accepted: 3 July 2026
Published: 4 July 2026

Copyright: © 2026 by the authors. Licensee MDPI, Basel, Switzerland. This article is an open access article distributed under the terms and conditions of the Creative Commons Attribution (CC BY) license.

1. Introduction

Marine pockmarks are negative micro-geomorphic landforms in deep-sea settings, formed by the combined action of fluid seepage, eruptive erosion and sediment reworking [1–3]. They provide critical seafloor indicators of cold seep activities [4], shallow fluid migration [5,6], gas hydrate dissociation and tectonic movements [7,8], and provide comprehensive records of the tectonic–sedimentary–fluid evolutionary processes of continental margins. Compared with isolated pockmarks, clustered pockmark groups provide a more robust reflection of deep fluid activity and stratigraphic stress evolution in local areas [9]. They are critical for deciphering regional tectonic activity, migration pathways of shallow hydrocarbons, occurrence conditions of gas hydrates, and evolutionary mechanisms of deep-sea sedimentary dynamics [10,11]. By altering seafloor topographic geometry,

pockmarks modify deep-sea current dynamics and sediment transport patterns, thereby modulating deep-sea geomorphic evolution, benthic ecological evolution and the occurrence of submarine geological hazards [12]. Therefore, pockmarks hold significant academic value for basic geological research, as well as applied value for marine resource exploration and marine engineering safety assurance.

Since their initial discovery in the North Atlantic, seafloor pockmarks have become a focal research topic across global marine geology, deep-sea fluid geology and the global carbon cycle [9,13]. Early studies primarily focused on geomorphological identification and qualitative characterization. With the widespread adoption of multibeam bathymetric technology, large-scale pockmark groups have been widely documented along passive continental margins and back-arc basins such as the North Sea [14,15], Norwegian Sea [16,17], Gulf of Mexico [18] and Mediterranean Sea [19,20]. Fluid seepage and gas release have been confirmed as the primary drivers of pockmark formation, and a preliminary relationship between pockmark morphology and fluid activity intensity has been preliminarily established [3,5]. With continuous advances in high-precision geophysical detection techniques, research has gradually shifted from macroscopic geomorphological recognition to detailed investigations into formation mechanisms, evolutionary processes and environmental effects [18,21]. Focusing on typical marine areas such as the Niger Delta of West Africa, the northwest Australian shelf and the North American Atlantic margin, previous studies have systematically revealed the combined controls exerted by tectonic faulting, sedimentary overpressure, sea-level fluctuation and gas hydrate dissociation on pockmark development [4,18,19]. The effects of fluid seepage from pockmarks on the marine carbon cycle, deep-sea cold seep ecosystems and seafloor geotechnical stability have also been thoroughly characterized, yielding a theoretical framework for pockmark evolution in passive continental margins.

As a typical marginal sea in the Western Pacific, the South China Sea hosts some of the most extensively distributed pockmarks and most active fluid systems globally, with its complex tectonics, diverse sedimentary systems and multiple genetic types of pockmarks [12,22,23]. Previous studies on pockmarks along the northern continental margin of the South China Sea and around the Guangle Uplift have yielded fruitful findings regarding morphological classification, fluid-driven genesis and sediment reworking effects, and verified close associations between pockmarks in the northwestern South China Sea and cold seep activities, bottom-current reworking as well as fault movements [24,25]. Numerous giant pockmarks and pockmark chains occur within the Xisha Sea area [12]. Some pockmarks are connected to form submarine channels through bottom current erosion, which has substantially reshaped the regional deep-sea geomorphology.

The present study investigates a typical pockmark group in the northwestern Xisha Uplift. Based on high-resolution multibeam bathymetric data, high-precision seismic reflection data and sediment core samples, this study characterizes the spatial distribution, morphometric characteristics and assemblage patterns of the local pockmark group. Integrated with the regional geological structure, sedimentary evolution and fluid activity background, the major controlling factors governing the formation and evolution of the pockmark group are systematically examined, and a dynamic evolutionary model for the pockmark group is constructed. The findings will advance the theoretical framework of pockmark research in the northwestern South China Sea and address the current research gap regarding detailed pockmark groups in the northwestern Xisha Uplift.

2. Stratigraphic Background

The South China Sea is located at the junction of the Eurasian, Pacific and Indo-Australian plates [26]. Its tectonic evolution has spanned three major tectonic cycles: the rifting stage from the Late Cretaceous to the Early Oligocene, the seafloor spreading stage from the Late Oligocene to the Early Miocene, and the regional subsidence stage since the Middle Miocene [27–29]. The northwestern continental margin of the South China Sea, which hosts the study area, lies along the collisional suture zone between the Indochina Block and the South China Block. Controlled by the combined effects of the East Vietnam Boundary Fault Zone, the Red River Fault Zone and the South China Sea Basin spreading, the margin features complex tectonic activities (Figure 1). The spreading of the South China Sea Basin from the Late Oligocene to the Early Miocene induced large-scale rifting on the northern continental margin, resulting in the development of a series of graben and half-graben structures [30–33]. Since the Middle Miocene, following the cessation of seafloor spreading, the region entered a thermal subsidence stage marked by markedly accelerated sedimentation rates [34–36]. The deposition of extremely thick marine strata has provided an abundant material basis for the generation and migration of shallow fluids. The continuous activity of deep-seated faults in the region links deep source rocks to shallow sedimentary layers, creating effective fluid migration pathways and providing favorable tectonic conditions for the development of seafloor pockmarks.

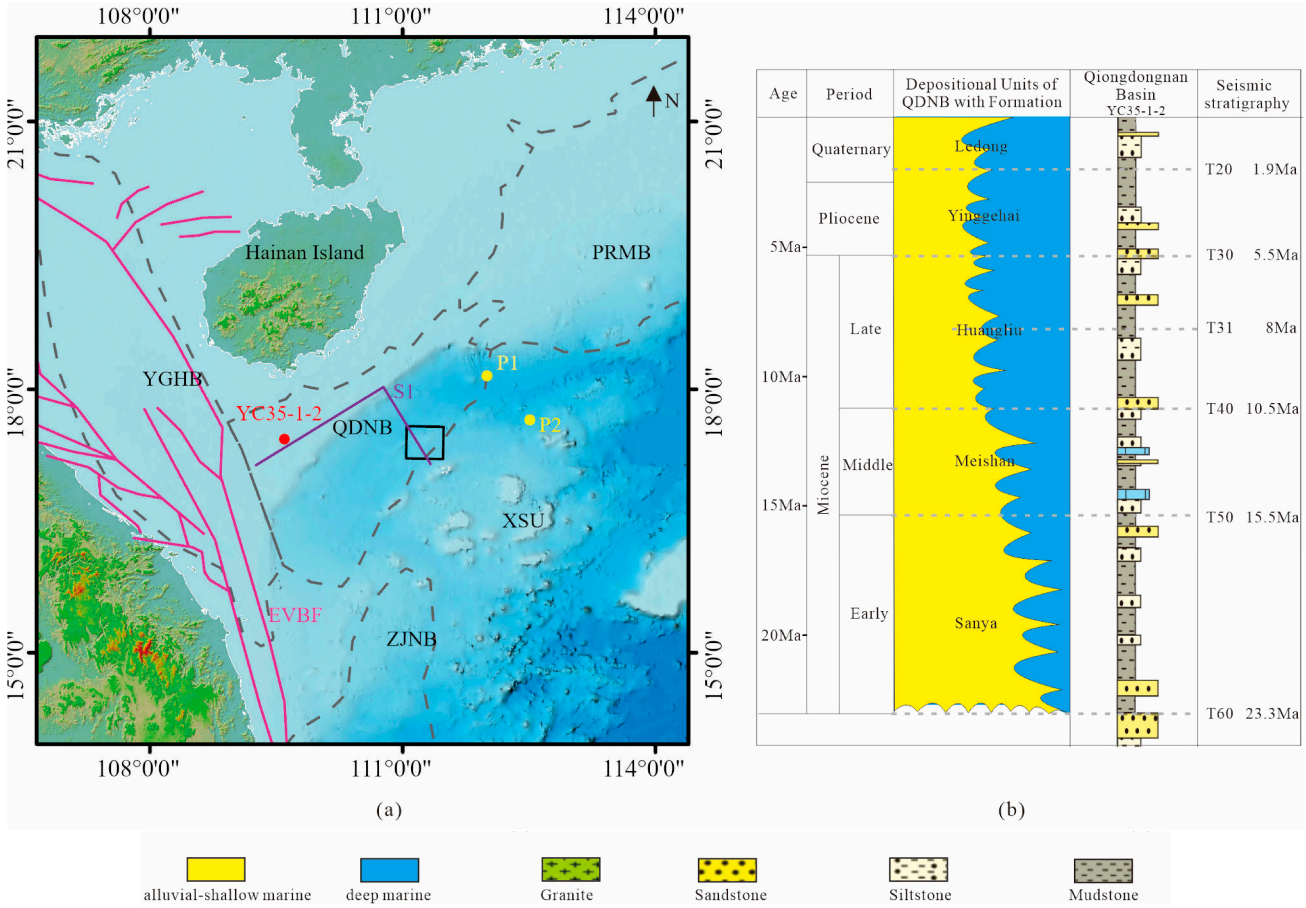


Figure 1. Regional tectonic framework (**a**) and stratigraphic division of the study area (**b**). The black box indicates the study area, the solid red circle marks the location of Well YC35-1-2, purple lines represent the tracks of long seismic section S1, gray dashed lines denote basin boundaries, solid red lines stand for fault zones, and solid yellow circles show sampling stations for sediment cores. YGHB, Yinggehai Basin; QDNB, Qiongdongnan Basin; XSU, Xisha Uplift; ZJNB, Zhongjiannan Basin; PRMB, Pearl River Mouth Basin; EVBF, East Vietnam Boundary Fault.

The Xisha Uplift is a long-lived large-scale Precambrian crystalline basement uplift along the northwestern continental margin of the South China Sea [37]. It is bordered by the Qiongdongnan Basin to the north, the Yinggehai Basin to the west, the Zhongjiannan Basin to the south, and the Pearl River Mouth Basin to the east, and constitutes as a key tectonic unit separating the northern continental shelf basins from the central deep-sea basin of the South China Sea (Figure 1). The Xisha Uplift originated during the Precambrian [38]. During the Paleogene, influenced by South China Sea rifiting, faulting occurred along the uplift margins, giving rise to a series of secondary sags and uplifts. During the Early Miocene seafloor spreading period, the entire uplift was submerged and accumulated widespread carbonate deposition [39]. Since the Middle Miocene, amid regional thermal subsidence, the uplift area has continued to sink, causing the gradual drowning of carbonate platforms, which are now capped by thick sequences of deep-sea mudstone [30,40].

The study area is located in the transitional zone between the northwestern Xisha Uplift and the southern Qiongdongnan Basin, geomorphologically forming a gentle slope dipping gradually from the Xisha Uplift toward the Qiongdongnan Basin. The strata in the study area are well developed, consisting of Paleogene, Neogene and Quaternary sequences from bottom to top, with the Neogene and Quaternary being the main horizons hosting pockmark groups. Based on drilling data from Well YC35-1-2 [41] in the Qiongdongnan Basin and high-resolution seismic reflection data, the Cenozoic strata in the study area can be divided into six major seismic sequences corresponding to six stratigraphic units, bounded by sequence boundaries at T60 (23.3 Ma), T50 (15.5 Ma), T40 (10.5 Ma), T31 (8 Ma), T30 (5.5 Ma) and T20 (1.9 Ma) [40,42], respectively (Figure 2). The Lower Miocene Sanya Formation was deposited in an alluvial to shallow marine setting. This formation is relatively thin across the Xisha Uplift area and thickens gradually toward the Qiongdongnan Basin. The Middle Miocene Meishan Formation formed in a shallow to bathyal marine environment. During the deposition of the Meishan Formation, carbonate platforms were extensively developed in the Xisha Uplift area, accumulating thick limestone and dolomite, whereas slope zones along the uplift margins were dominated by clastic deposits. Numerous reefs and shoals are developed in this formation, which are characterized by high porosity and permeability. The Upper Miocene Huangliu Formation was deposited in a bathyal to abyssal marine setting. During the deposition of the Huangliu Formation, regional tectonic activity weakened, sedimentation rates accelerated, and stratigraphic thickness remained stable. The Pliocene Yinggehai Formation formed in an abyssal marine environment. During the deposition of the Yinggehai Formation, the entire region was in a rapid subsidence stage. Abundant slump structures and turbidites are developed in this formation, reflecting the instability of the regional sedimentary environment. The Quaternary Ledong Formation was deposited in an abyssal marine environment. The high sedimentation rate of the Ledong Formation has resulted in undercompaction of the strata and elevated pore water pressure, which readily promotes the formation of shallow overpressure and provides the driving force for fluid seepage and pockmark formation.

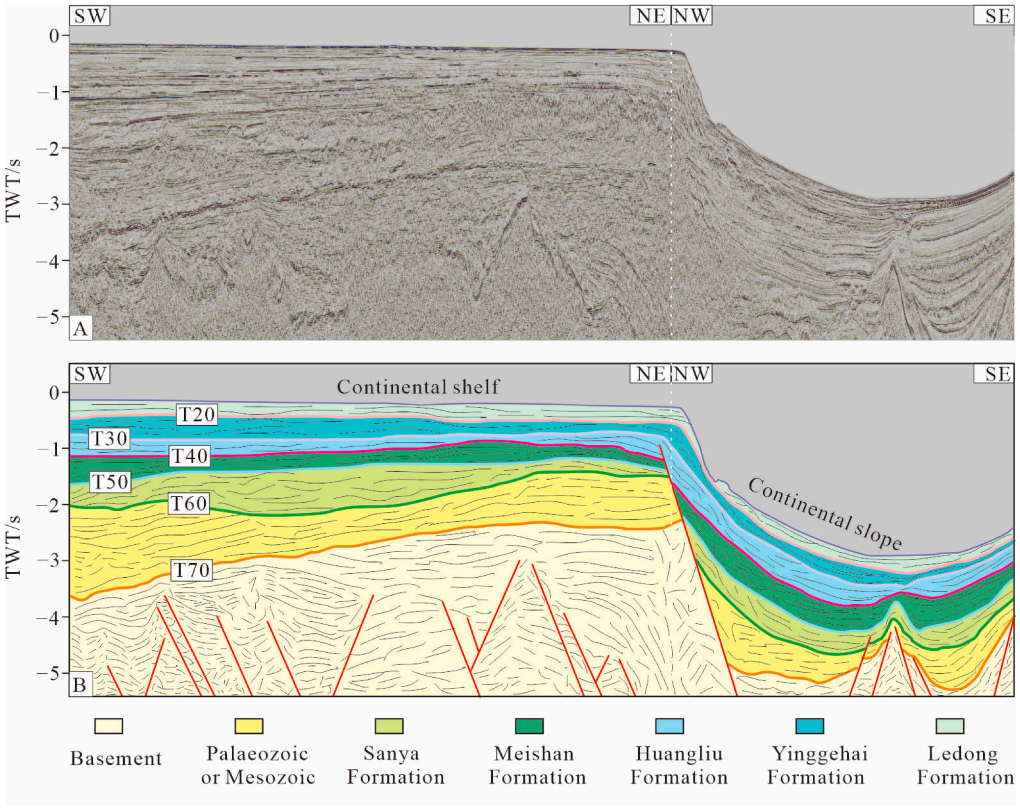


Figure 2. Seismic section S1 showing Cenozoic seismic sequences and stratigraphic framework. The profile location is presented in Figure 1. The red solid lines represent faults.

3. Data and Methods

The data used in the present study consist of high-resolution multibeam bathymetric data, multi-channel seismic reflection data, and seafloor sediment core samples, all acquired and provided by the Guangzhou Marine Geological Survey (GMGS).

3.1. Data

The research dataset comprises high-resolution multibeam bathymetric data, multi-channel reflection seismic data, and sediment core samples collected from the seafloor. Three data types were integrated to characterize the morphology and stratigraphic architecture of the pockmark field in the northwestern Xisha Uplift, and to elucidate the underlying evolutionary mechanisms.

The multibeam bathymetric data were processed to a final grid resolution of 50 m × 50 m, which enables precise identification of seafloor micro-topographic features within the study area. This resolution is sufficient to delineate pockmark boundaries, extract morphometric parameters, and perform spatial distribution statistics. The dataset provides complete coverage of the study block in the northwestern Xisha Uplift, featuring high bathymetric accuracy and good topographic continuity, thereby avoiding issues such as topographic distortion and data gaps commonly associated with deep-water surveys. Based on the multibeam data, morphometric parameters including pockmark diameter, depth, floor gradient, and rim geometry were extracted for systematic analysis of the pockmark field distribution.

The 2D multi-channel reflection seismic data exhibit a high signal-to-noise ratio and well-resolved stratigraphic reflection characteristics, enabling the identification of fault structures, overpressure zones, and anomalous fluid bodies within the pockmark-bearing strata. The seismic exploration depth encompasses the entire Cenozoic sedimentary suc-

cession, providing a comprehensive view of the stratigraphic architecture, fault geometry, deep-seated fluid migration pathways, and sub-pockmark stratigraphic responses in the study area.

Sediment core sampling was performed in depositional zones surrounding the pockmark development area. The recovered cores were used to determine the lithology and grain-size parameters of surrounding sediments, to identify variations in depositional environment, hydrodynamic conditions, and post-depositional reworking characteristics associated with pockmark formation.

3.2. Analytical Methods

Multibeam raw data were first subjected to a series of pre-processing procedures, including depth correction, tidal correction, sound velocity correction, and outlier removal, to eliminate systematic biases introduced by environmental factors and instrumental errors. The corrected data were subsequently gridded to generate a high-resolution seafloor topographic model at 50 m × 50 m resolution. Using standard criteria for seafloor micro-geomorphology identification, individual pockmarks were recognized and their boundaries precisely delineated. Morphometric parameters—including major axis length, minor axis length, depth, area, volume, and slope—were batch-extracted for each pockmark, enabling a systematic analysis of the spatial distribution characteristics of the pockmark field.

Multi-channel seismic data interpretation was conducted using the Petrel 2018 software platform. Detailed analysis of strata beneath pockmarks was performed using amplitude, frequency, and seismic facies attributes, to identify geological features genetically related to pockmark formation, including fluid seepage conduits, stratigraphic disturbances, and anomalous reflections. The controlling factors governing pockmark development were analyzed in conjunction with the regional tectonic evolution history.

For the sediment cores, detailed visual descriptions were first recorded, documenting color, lithological composition, sedimentary structure, bedding type, and bioturbation or physical disturbance features. Grain-size analysis was subsequently performed: samples were pre-treated by oven-drying, disaggregation, organic matter removal, and carbonate dissolution, then analyzed using a laser diffraction particle size analyzer to obtain the proportions of clay, silt, and sand fractions, as well as grain-size statistical parameters including mean grain size, sorting coefficient, skewness, and kurtosis. By comparing grain-size characteristics across different sub-regions, the sediment transport and depositional dynamic environments were interpreted, and the influence of contour current reworking and sedimentary infilling on the formation, modification, and preservation of pockmarks were assessed.

4. Results

4.1. Multibeam Bathymetric Data Analysis

The study area features a topographic pattern characterized by deeper terrain in the northwest and shallower terrain in the southeast. Water depth gradually decreases by nearly 700 m from the northwest to the southeast, with an average seabed gradient of approximately 3.2°. A prominent topographic steep zone develops in the middle of the slope, where slope gradients increase sharply, serving as the primary topographic setting for the development of pockmark group. Three geomorphic units are classified based on seabed topography in the study area. The northwestern abyssal plain (water depth > 1600 m), a flat terrain with slopes less than 1°; central slope transition zone (water depth 1200–1600 m), intense topographic undulation and highly variable slopes, representing the concentrated distribution zone of the pockmark group; the southeastern

platform margin (water depth < 1200 m), gentle terrain that gradually transitions toward the main body of the Xisha Uplift (Figure 3).

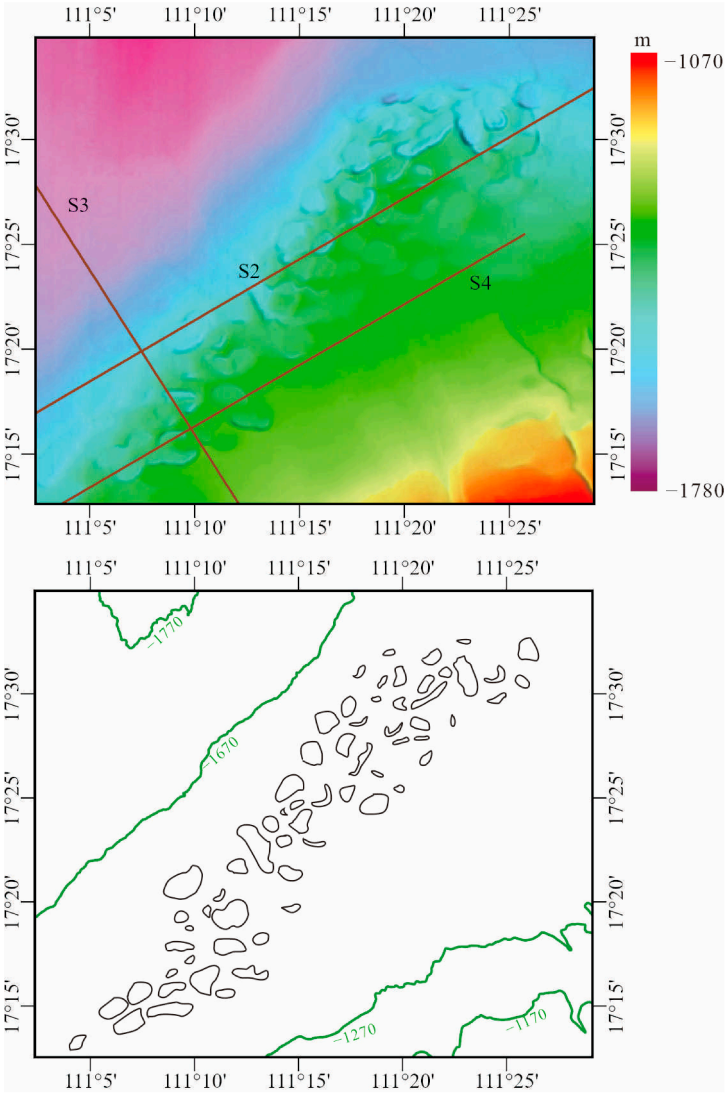


Figure 3. (**Upper panel**): bathymetric and geomorphological map of the study area, where the brown solid lines indicate the locations of three seismic sections; (**lower panel**): distribution of identified pockmarks.

4.1.1. Spatial Distribution Characteristics of Pockmark Cluster

A total of 64 pockmarks are identified using multibeam bathymetric datasets (Figure 3). Spatially, these pockmarks exhibit a NE–SW zonal distribution, consistent with the regional structural trend and the strike of the seabed slope. This pockmark group is predominantly concentrated within the central slope transition zone, with the vast majority confined to the 1300–1500 m depth range.

Pockmarks reach their densest concentration in the central part of the study area, with an average density of 0.8 pockmarks per square kilometer. In contrast, pockmark abundance declines markedly at the northern and southern extremities, where densities drop below 0.4 pockmarks/km^2. Pockmark distribution shows a significant positive correlation with seabed slope: nearly all pockmarks form within the steep topographic zone where slopes exceed 5° (Figure 4), whereas flat areas with slopes < 2° are almost devoid of pockmarks.

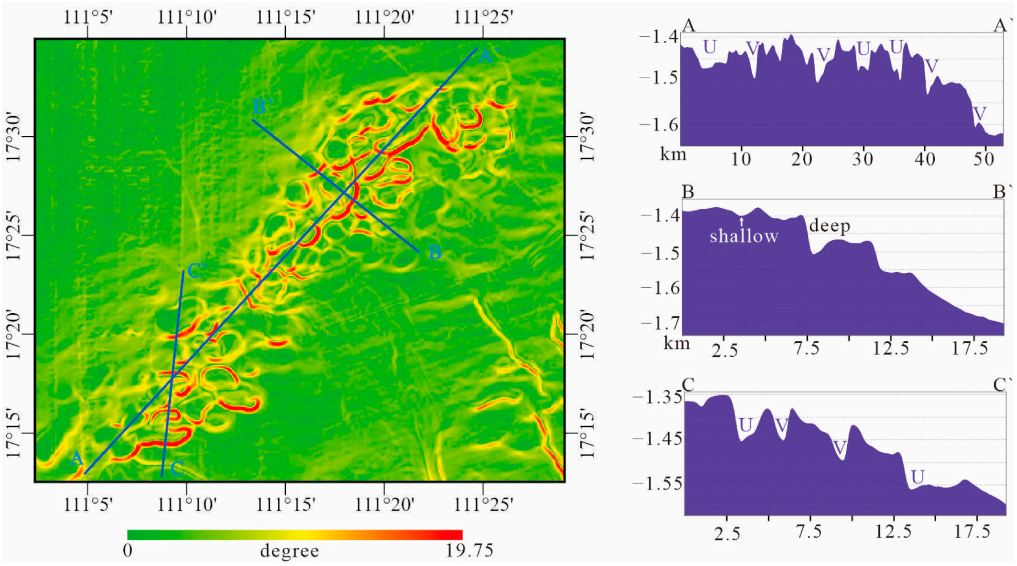


Figure 4. (**Left panel**): seabed slope map of the study area; (**right panel**): bathymetric variations along three profiles, whose locations are shown in the left panel.

Pockmarks display diverse cross-sectional morphologies, ranging from simple single depressions to complex composite pockmarks. Obvious spatial variations exist in pockmark depth and dimension, the largest and deepest pockmarks occur in the central zone, with dimensions gradually diminishing toward the northern and southern ends, consistent with the spatial density pattern of the pockmark group. The overall terrain of the pockmark group area is characterized by alternating peaks and troughs. U-shaped and V-shaped pockmarks are recognized. U-shaped pockmarks feature flat bottoms and gentle sidewalls, typically corresponding to circular or oval plan-view geometries. V-shaped pockmarks possess sharp bottoms and steep sidewalls, generally representing elongated pockmarks. U-shaped and V-shaped depressions alternate spatially across the study area (Figure 4).

4.1.2. Morphological Classification and Statistical Parameters of Pockmarks

Based on plan-view morphology, pockmarks in the study area are classified into three primary types: circular and elliptical, crescentic, and elongated (Figure 5). Statistical morphological parameters for each category are summarized in Table 1.

Table 1. Main morphological parameters of pockmarks.

Shape	Long-Axis Diameter/km	Short-Axis Diameter/km	Depth/m	Number
Circular and Elliptical	0.86–2.15	0.69–1.95	11–122	32
Crescent-Shaped	1.15–3.81	0.56–2.29	19–114	13
Elongated	0.92–4.74	0.57–1.23	33–137	19
Shape	**Volume/10^6 m^3**	**Surface Area/km^2**	**Perimeter/km**	**Orientation/°**
Circular and Elliptical	4.9–286.7	0.47–3.28	2.44–8.56	15°~78°
Crescent-Shaped	5.4–313.5	0.53–3.34	2.71–7.35	22°~85°
Elongated	4.2–386.9	0.26–4.02	1.99–9.93	30°~92°

Circular and elliptical pockmarks constitute the most abundant type, with a total count of 32. These pockmarks exhibit regular, circular or sub-oval planforms with distinct boundaries and relatively steep walls. Their long-axis diameters range from 0.86 km to 2.15 km (mean = 1.42 km), while short-axis diameters vary between 0.69 km and 1.95 km

(mean = 1.21 km). Pockmark depths range widely from 11 m to 122 m, with an average depth of 68 m. The strikes of circular and oval pockmarks are predominantly oriented between 15° and 78°, consistent with the regional structural trend.

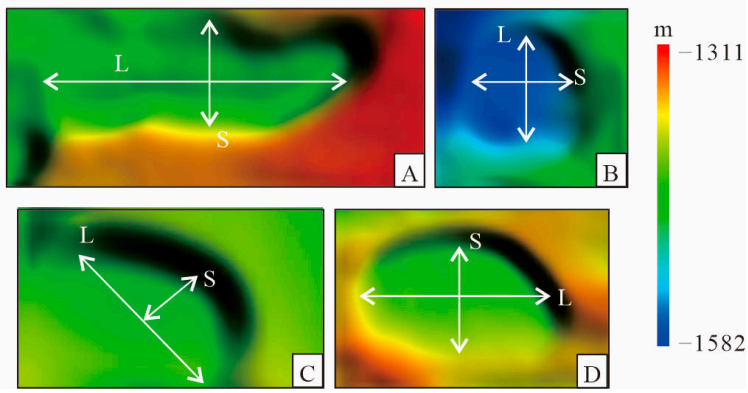


Figure 5. Planar characteristics of circular–elliptical, crescentic and elongated pockmarks. (**A**): elongated pockmark; (**B**): circular pockmark; (**C**): crescentic pockmark; (**D**): elliptical pockmark. The long white line denotes the major axis (L), and the short white line denotes the minor axis (S).

Thirteen crescentic pockmarks are identified, displaying crescent or horseshoe planforms with a distinct opening direction and asymmetric walls: the wall adjacent to the opening is gentle, while the opposite wall is steep. Long-axis diameters span 1.15–3.81 km (mean = 2.34 km), short-axis diameters range 0.56–2.29 km (mean = 1.32 km), and length-to-width ratios fall between 1.5 and 2.5. Depths vary from 19 m to 114 m, with a mean depth of 72 m. Crescentic pockmarks strike primarily from 22° to 85°, and their openings mostly face northwest or southeast.

Nineteen elongated pockmarks are identified, characterized by strip-like or irregular oval planforms. Long-axis diameters range 0.92–4.74 km (mean = 2.68 km), short-axis diameters vary 0.57–1.23 km (mean = 0.89 km), and length-to-width ratios range from 2.0 to 5.0. Depths extend from 33 m to 137 m, with an average depth of 85 m—representing the deepest average depth among the three pockmark types. Elongated pockmarks strike mainly between 30° and 92°, highly consistent with the strike of regional faults.

4.2. Multi-Channel Seismic Data Analysis

Interpretations were conducted on three multi-channel seismic sections covering the study area to analyze the seismic facies characteristics of strata underlying concentrated pockmark zone. Bounded by the regional unconformity T40, the sedimentary succession can be vertically divided into two sequences. A variety of anomalous seismic facies directly linked to fluid activity are developed within the shallow hemipelagic deposits, providing critical seismological evidence for the genetic analysis of pockmarks.

4.2.1. Seismic Facies of Deep Basement and Carbonate Uplifts Below Interface T40

Strata beneath the T40 interface constitute the basement structural layer of the study area, and is further subdivided into a lower deep-water calcareous mudstone member and an upper carbonate uplift member from bottom to top. The lowermost succession consists of Oligocene to Middle Miocene calcilutites, featuring low-amplitude chaotic seismic facies with highly discontinuous seismic reflectors, strong lateral amplitude variations, and locally scattered high-amplitude reflection patches (Figure 6). This succession was deposited under tectonically active conditions during the South China Sea spreading phase, reflecting unstable sedimentary environments.

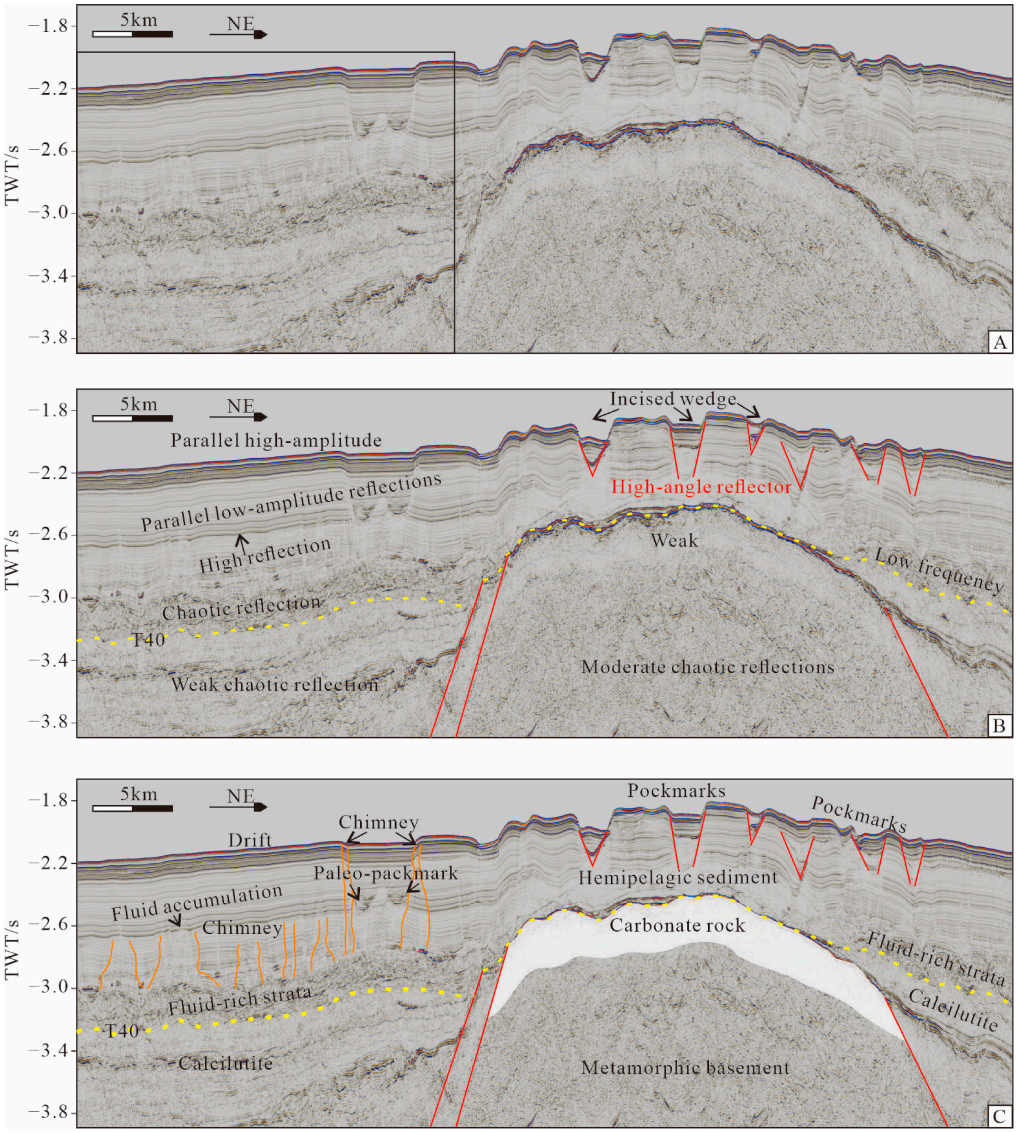


Figure 6. Seismic facies characteristics of seismic section S2. The profile location is shown in Figure 3. (**A**): original seismic section; (**B**): interpretation of distinctive seismic facies; (**C**): geological and sedimentary facies interpretation. Solid red lines denote faults.

Large-scale carbonate uplifts developed within the calcilutite succession constitute the core geological bodies underlying pockmarks. The crest of each uplift is marked by a continuous high-amplitude reflection horizon corresponding to the T40 unconformity, which records the carbonate platform drowning event triggered by rapid sea-level rise at the end of the Middle Miocene. The interior of carbonate uplifts exhibits transparent-to-chaotic seismic facies with no distinct bedding structures; locally identified intermittent mound-shaped high-amplitude reflectors indicate reef–shoal facies formed under high-energy conditions within the paleo-platform (Figure 7). The flanks of the uplifts are characterized by ramp reflections dipping toward adjacent depressions, where seismic reflections gradually converge and grade into chaotic reflections of the underlying calcareous mudstones, recording lateral facies transitions from carbonate platforms to basin settings.

Karst-fracture systems developed on the crests and flanks of carbonate uplifts serve as both fluid storage spaces and lateral migration conduits for subsurface fluids. On seismic sections, these systems manifest as chaotic reflective zones marked by abrupt amplitude shifts, distorted seismic events, and phase reversals. Such fracture networks

channel dispersed fluids ascending along deep major faults toward uplift crests, generating regionally extensive zones of anomalous fluid overpressure.

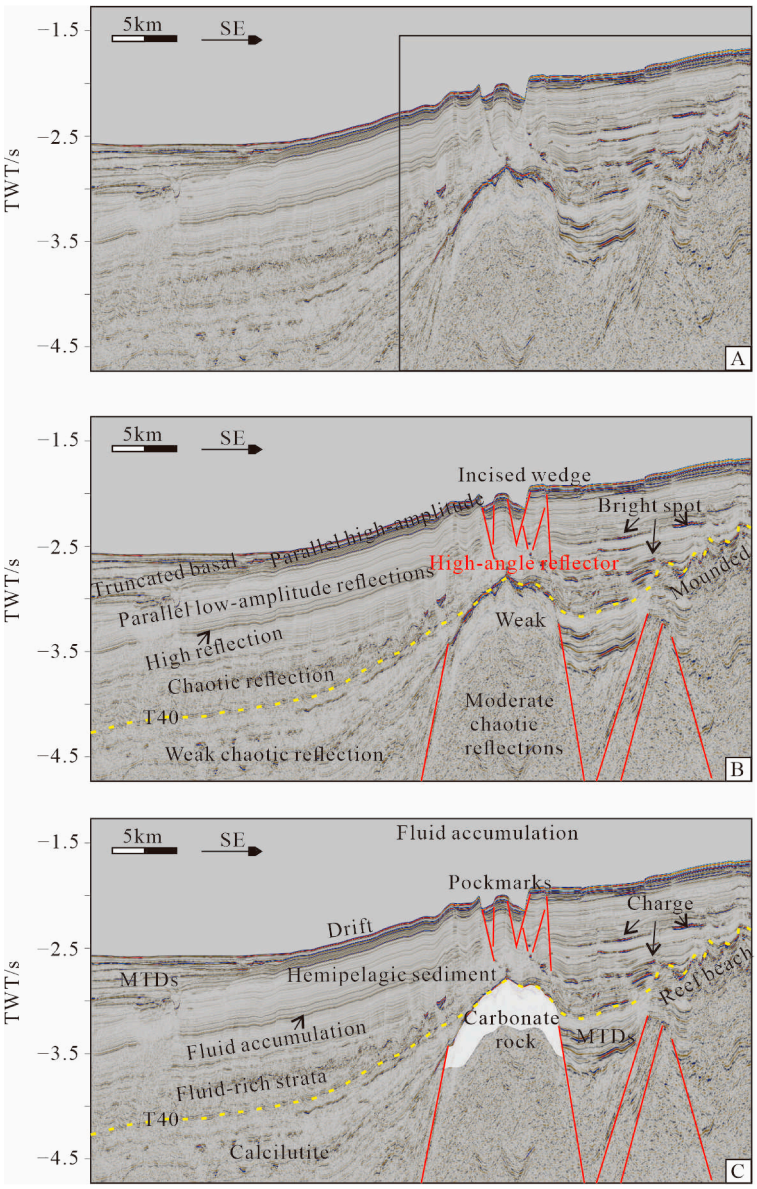


Figure 7. Seismic facies characteristics of seismic section S3. The profile location is shown in Figure 3. (**A**): original seismic section; (**B**): interpretation of distinctive seismic facies; (**C**): geological and sedimentary facies interpretation. Solid red lines denote faults.

4.2.2. Seismic Facies of Overlying Hemipelagic Deposits Above Interface T40

Strata above the T40 interface correspond to Late Miocene and younger hemipelagic sediments, displaying parallel to subparallel, moderate-amplitude continuous seismic facies with laterally stable reflectors and negligible tectonic deformation. This seismic signature indicates that the study area entered a tectonically quiescent phase after the late Middle Miocene, dominated by sustained fine-grained hemipelagic sedimentation (Figure 6).

Thickness of this hemipelagic succession exhibits prominent spatial heterogeneity: it thins dramatically over carbonate uplift crests and progressively thickens toward peripheral depressions. This thickness variability is directly controlled by paleotopographic relief of the underlying carbonate uplifts.

The hemipelagic succession is primarily composed of silty mudstones and argillaceous siltstones, featuring low porosity and low permeability that collectively form an effective regional seal. This low-permeability seal impedes upward fluid escape from deep formations, resulting in prolonged fluid accumulation and overpressure buildup at the base of the seal. Once fluid pressure exceeds the tensile strength of overlying sediments, massive fluid expulsion occurs via hydraulic fracturing of the seal, ultimately generating pockmark depressions on the seafloor.

4.2.3. Anomalous Seismic Facies Associated with Fluid Activity

Three types of fluid-related anomalous seismic facies were identified within hemipelagic strata underlying pockmarks: high-amplitude reflectors, bright spots, and high-angle reflectors.

High-amplitude reflectors represent the diagnostic seismic indicator of fluid overpressure accumulation. They occur as layered or patchy continuous high-amplitude bodies locally embedded within hemipelagic sequences, with markedly stronger reflection amplitudes relative to overlying normal hemipelagic deposits and prominent seismic contrasts between the two units. These high-amplitude bodies extend laterally for hundreds of meters to several kilometers, distributed in NE–SW trending bands that perfectly match the strike of underlying carbonate uplifts and the spatial distribution of pockmark groups. Characterized by high amplitude, low frequency and high continuity (Figures 6 and 7), high-amplitude reflectors mark widespread fluid layers formed by lateral fluid migration and pooling at the base of the regional seal.

Bright spots constitute a direct seismic indicator of shallow fluid accumulation, appearing as isolated local high-amplitude anomalies associated with reflection pull-down. Their reflection amplitudes typically reach 3–5 times those of surrounding host sediments. After breaking through deep overpressure zones, ascending fluids continue migrating upward and form small-scale fluid accumulations within shallow sediments, generating bright spot anomalies (Figure 7).

High-angle reflectors serve as a diagnostic seismic identifier for pockmarks, manifested as steeply dipping high-amplitude reflective belts along pockmark sidewalls that clearly delineate V- or U-shaped pockmark boundaries within strata. Dips of high-angle reflectors in the study area predominantly range from 45° to 75°, and their vertical penetration depth directly records the incision depth of corresponding pockmarks. These reflectors exhibit stronger amplitudes than other topographic break zones on the seafloor, with vertical extents substantially greater than the bathymetric depth of pockmarks. This observation demonstrates that high-angle reflectors do not merely represent topographic boundaries, but act as robust proxies for fluid migration along pockmark flanks.

5. Discussion

5.1. Controls of Surface Sedimentary Characteristics on Pockmark Development

Lithology, grain-size composition, compaction state of surface sediments and sedimentary dynamic conditions constitute the critical shallow geological factors governing the spatial occurrence, morphological differentiation and distribution pattern of pockmarks. A complete sedimentary environmental gradient extends from the southeastern uplift to the northwestern abyssal plain in the study area, corresponding to three geomorphic units: the marginal platform of the Xisha Uplift, the central slope transition zone and the northwestern abyssal plain, where prominent spatial heterogeneities exist in sediment grain size, sedimentation rate and stratigraphic compaction.

The southeastern marginal platform lies at water depths shallower than 1200 m, featuring gentle topography with seabed gradients generally less than 2° and stable regional hydrodynamic conditions dominated by slow deposition of fine-grained silty clay. Con-

tinuous compaction yields highly compacted strata with balanced pore water pressure, precluding substantial overpressure accumulation. Meanwhile, stable bottom currents barely erode or remodel surficial sediments, resulting in nearly absent pockmarks in this zone. Compared with the slope belt, sediments on the marginal platform exhibit better sorting and homogeneous stratigraphic architecture, which inhibits the generation of local weak stress zones and restrains pockmark initiation and development from the perspective of the sedimentary medium.

The slope transition zone represents the core area of concentrated pockmark development and hosts the most remarkable variability in surficial sedimentary environments. This zone is characterized by a steepened seabed gradient, complex hydrodynamic regimes, frequent bottom current scouring and sediment slumping, with sedimentary sequences dominated by interbedded heterogeneous clayey silt and thin turbidite layers. Grain-size analyses reveal alternating clay and silt fractions, poor sorting coefficients and intense lateral stratigraphic heterogeneity, generating abundant local weak structural planes (Figure 8). Furthermore, the Quaternary Ledong Formation accumulated at a high sedimentation rate; rapid accumulation of fine-grained sediments led to insufficient stratigraphic compaction and impeded pore water drainage, resulting in persistent shallow overpressure. This provides the essential driving force for upward migration of deep fluids and their breakthrough through shallow strata.

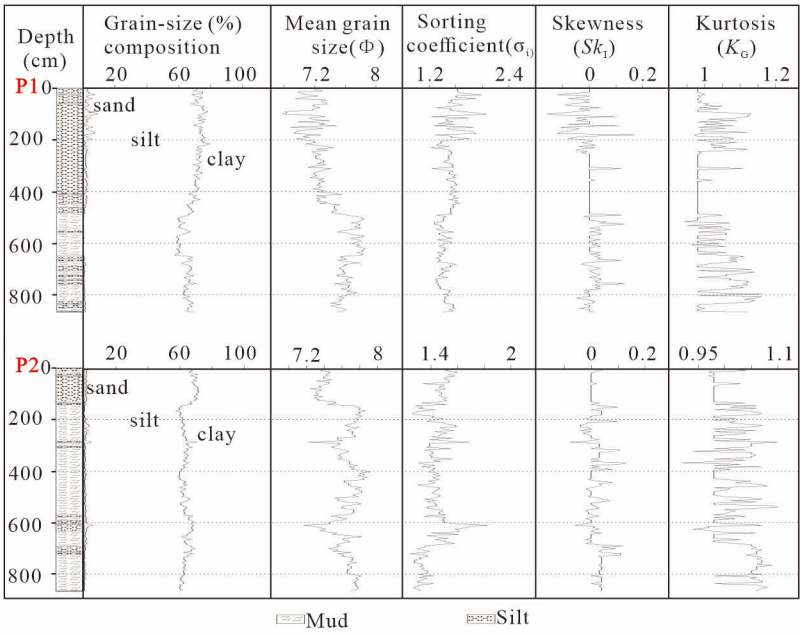


Figure 8. Grain-size parameters and sediment composition of seafloor surface sediments. The profile locations are shown in Figure 1.

The abyssal plain features flat terrain with gradients below 1°. Despite thick sedimentary sequences and pervasive shallow overpressure, homogeneous sediments and intact overall stratigraphy hinder the formation of focused fluid migration pathways, with only scattered, small, shallow pockmarks observed. Additionally, differential sedimentary remolding across the central slope directly controls pockmark morphological differentiation. U-shaped pockmarks occur in regions with relatively homogeneous sediments and mild bottom current modification, formed by uniform fluid seepage that generates flat-bottomed, gently walled geomorphology. V-shaped and elongated pockmarks prevail in turbidite-rich zones with fractured stratigraphic frameworks; rapid fluid eruption coupled with directional bottom current erosion produces deep-cut landforms with steep walls and sharp bottoms. Crescentic pockmarks are entirely governed by lateral bottom current

remolding: following initial pockmark formation via fluid expulsion, persistent unidirectional bottom currents scour one side of the depression, yielding distinctive asymmetric open morphologies.

5.2. Fluid Escape Processes and Dynamic Evolution Mechanisms of Pockmark Group

The generation and evolution of pockmark groups in the study area represent a dynamic coupling process involving deep tectono-fluid activities, intermediate reservoir systems and shallow sedimentary caprocks (Figure 9). The complete evolutionary sequence can be subdivided into three stages: fluid accumulation, hydraulic fracturing and incipient pockmark formation, and bottom current remolding with morphological differentiation. Spatiotemporal variations in deep fluid escape account for the diverse distribution patterns and morphologies of pockmark group across the study area. The unique sequence-stratigraphic architecture provides a full set of geological carriers for fluid migration, accumulation and expulsion.

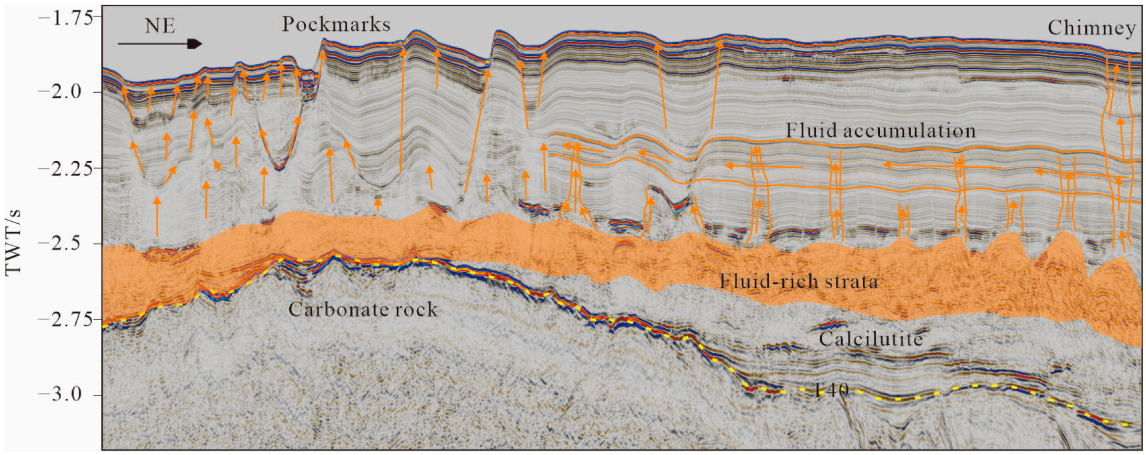


Figure 9. Fluid migration processes in pockmark-bearing strata, orange arrows denote fluid migration pathways. The location is shown at S4 in Figure 3.

Stage 1 Fluid Accumulation (Pre-Late Miocene): Extensive carbonate uplifts and karst-fracture systems developed beneath the T40 unconformity surface. Carbonate reef–shoal strata possess exceptionally high porosity and permeability, and, together with fractured fault zones, form a network for fluid storage and migration. Gas-bearing fluids generated by deep source rocks migrated upward continuously along deep-rooted major faults and accumulated within karst fissures atop carbonate uplifts, forming large-scale fluid overpressure bodies. Rapid sea-level rise during the terminal Middle Miocene induced complete submergence of the carbonate platform and the formation of the T40 unconformity, which acted as a critical sealing interface to prevent premature fluid loss.

Stage 2 Hydraulic Fracturing and Incipient Pockmark Formation: Since the Late Miocene, the study area entered a thermal subsidence phase. Persistently deposited hemipelagic fine-grained mudstones formed a regionally extensive low-permeability caprock that blocked vertical fluid escape pathways, enabling progressive buildup of fluid overpressure atop carbonate uplifts. Increasing overburden load from thickening sedimentary sequences drove pore fluid pressure to exceed the tensile strength of shallow caprock strata, triggering hydraulic fracturing and the development of high-angle fracture conduits. Rapid upward fluid eruption entrained fine-grained sediments to scour surficial seabed strata (Figure 10), creating embryonic pockmarks. Seismic high-amplitude reflectors, bright spot anomalies and high-angle reflection interfaces precisely record the successive

processes of fluid overpressure buildup, fracture propagation and fluid eruption during this stage.

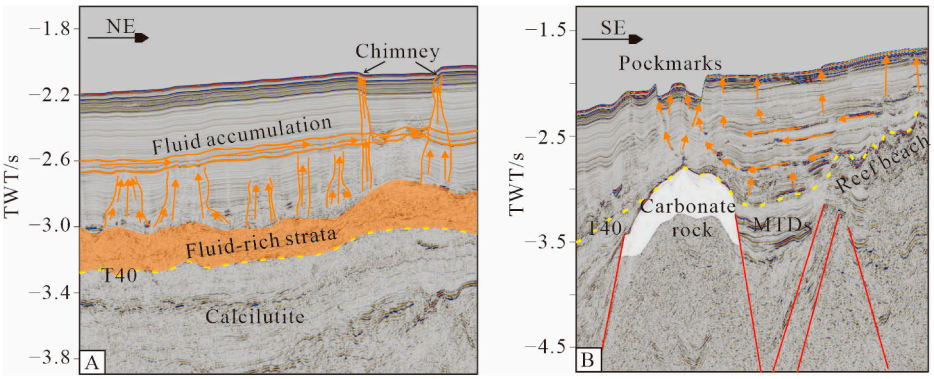


Figure 10. Fluid migration processes in pockmark-bearing strata, orange arrows denote fluid migration pathways, solid red lines denote faults. The (**A**) location is shown in the black box in Figure 6A, the (**B**) location is shown black box in Figure 7A.

Stage 3 Bottom Current Remolding and Morphological Differentiation: Incipient pockmarks alter local hydrodynamic fields through irregular seabed topography, enabling differential erosion and remolding of pockmark walls and floors by regional bottom currents parallel to the slope strike. Regular circular and elliptical pockmarks form where mild bottom currents uniformly remodel single depressions generated by one-off small-scale fluid eruptions. In zones with multi-stage superimposed fluid expulsion and densely developed fractures, adjacent small pockmarks coalesce to form large composite pockmarks. Sustained unidirectional bottom current scouring further reshapes depressions into crescentic and elongated morphologies. This stage dominates pockmark spatial differentiation, whereby fluid escape intensity, episodicity and bottom current modification jointly determine pockmark dimension, geometry and strike extension.

6. Conclusions

Based on integrated analysis of multi-source geological and geophysical data, this study systematically investigates the spatial distribution, morphological characteristics, seismic responses and genetic evolution of the pockmark group in the northwestern area of the Xisha Uplift.

(1) The study area consists of three geomorphic units: northwestern abyssal plain, central slope transition zone and southeastern platform margin. Pockmarks show prominent zonal aggregation. A total of 64 pockmarks are concentrated in the 1300–1500 m deep central steep slope zone, aligning zonally along the NE–SW structural strike. Their density and scale positively correlate with seabed gradient, while gentle slopes barely develop pockmarks. Seabed topographic gradient dominates the spatial distribution of local pockmarks.

(2) Vertical stratigraphic heterogeneity provides essential geological conditions for pockmark development. Carbonate uplifts and karst-fracture systems beneath the T40 unconformity serve as reservoirs and migration pathways for deep gas-bearing fluids. The overlying Late Miocene–Quaternary hemipelagic fine-grained sediments form a widespread low-permeability caprock, which restricts vertical fluid escape and induces sustained overpressure accumulation, constituting the primary driving force for pockmark formation. Three fluid-related seismic facies, including high-amplitude reflections, bright spot anomalies and high-angle reflectors, record the entire process of fluid accumulation, migration and seabed breakthrough for pockmark generation.

(3) Spatial heterogeneity of surface sedimentary environments controls pockmark morphological differentiation. The central slope transition zone features poorly sorted sediments and strong stratigraphic anisotropy. Rapid sedimentation of the Quaternary Ledong Formation causes undercompacted strata and extensive shallow overpressure, favoring fluid breakthrough and pockmark nucleation. The pockmark evolution undergoes three stages: pre-Late Miocene fluid accumulation, where hydrocarbon-bearing fluids migrate along faults and accumulate in carbonate karst fissures to form large-scale overpressure bodies; post-Late Miocene hydraulic fracturing and embryonic pockmark formation, where increased overburden pressure drives fluid eruption through fractured caprocks to form initial seabed depressions; and bottom-current reworking and morphological differentiation, where regional bottom currents erode, reshape and merge embryonic pockmarks, eventually forming the diversified and regularly distributed pockmark geomorphology in the study area.

Author Contributions: Conceptualization, Investigation, Data Curation, and Methodology, T.L. and X.L.; Writing—Original Draft, T.L. and Y.Y.; Writing—Review and Editing, L.W. and X.L.; Investigation, L.H. and X.B.; Software, T.L. All authors have read and agreed to the published version of the manuscript.

Funding: This research was funded by the Project of Sanya Yazhou Bay Science and Technology City (grant number SCKJ-JYRC-2025-04), the Sanya Science and Technology Innovation Special Project (grant number 2022KJCX13), the 2025 Hainan Province "South China Sea New Star" Science and Technology Innovation Talent Platform Project (grant number NHXXKJCX202542), and the China Geological Survey Project (grant number DD202603102602).

Data Availability Statement: All data have been provided in this paper. Further inquiries can be directed to the corresponding authors.

Acknowledgments: We would like to express our sincere gratitude to the Guangzhou Marine Geological Survey for generously providing essential multibeam bathymetric, seismic and geological foundational data, without which this research could not have been carried out smoothly.

Conflicts of Interest: The authors declare no conflicts of interest.

References

1. Judd, A.; Hovland, M. *Seabed Fluid Flow: The Impact on Geology, Biology and the Marine Environment*; Cambridge University Press: Cambridge, UK, 2009.
2. Hovland, M.; Gardner, J.V.; Judd, A. The Significance of Pockmarks to Understanding Fluid Flow Processes and Geohazards. *Geofluids* **2002**, *2*, 127–136. [CrossRef]
3. Vaknin, I.; Aharonov, E.; Holtzman, R.; Katz, O. Gas Seepage and Pockmark Formation From Subsurface Reservoirs: Insights From Table-Top Experiments. *J. Geophys. Res. Solid Earth* **2024**, *129*, e2023JB028255. [CrossRef]
4. Sergiou, S.; Ntrouva, D.; Geraga, M.; Christodoulou, D.; Papatheodorou, G. Lithological and Geochemical Differentiations in an Urbanized, Shallow Marine Cold-Seep Environment. The Case of Patras Gulf Active Pockmark Field. *Cont. Shelf Res.* **2026**, *296*, 105583. [CrossRef]
5. Callow, B.; Bull, J.; Provenzano, G.; Böttner, C.; Birinci, H.; Robinson, A.; Henstock, T.; Minshull, T.; Bayrakci, G.; Lichtschlag, A. Seismic Chimney Characterisation in the North Sea—Implications for Pockmark Formation and Shallow Gas Migration. *Mar. Pet. Geol.* **2021**, *133*, 105301.
6. Maia, A.; Cartwright, J.; Andersen, E. Shallow Plumbing Systems Inferred from Spatial Analysis of Pockmark Arrays. *Mar. Pet. Geol.* **2016**, *77*, 865–881. [CrossRef]
7. Luo, M.; Chen, L.; Tong, H.; Yan, W.; Chen, D. Gas Hydrate Occurrence Inferred from Dissolved Cl- Concentrations and δ18O Values of Pore Water and Dissolved Sulfate in the Shallow Sediments of the Pockmark Field in South-western Xisha Uplift, Northern South China Sea. *Energies* **2014**, *7*, 3886–3899. [CrossRef]
8. Betzler, C.; Lindhorst, S.; Hübscher, C.; Lüdmann, T.; Fürstenau, J.; Reijmer, J. Giant Pockmarks in a Carbonate Platform (Maldives, Indian Ocean). *Mar. Geol.* **2011**, *289*, 1–16. [CrossRef]
9. Hovland, M.; Talbot, M.R.; Qvale, H.; Olaussen, S.; Aasberg, L. Methane-Related Carbonate Cements in Pockmarks of the North Sea. *J. Sediment. Res.* **1987**, *57*, 881–892. [CrossRef]

10. Xiong, P.; Cheng, C.; Kuang, Z.; Ren, J.; Liang, J.; Lai, H.; Chen, Z.; Lu, J.; Fang, X.; Jiang, T. Sedimentary Characteristics and Genetic Mechanism of the Giant Ancient Pockmarks in the Qiongdongnan Basin, Northern South China Sea. *Acta Oceanol. Sin.* **2023**, *42*, 120–133. [CrossRef]
11. Panieri, G.; Bünz, S.; Fornari, D.; Escartin, J.; Serov, P.; Jansson, P.; Torres, M.; Johnson, J.; Hong, W.; Sauer, S. An Integrated View of the Methane System in the Pockmarks at Vestnesa Ridge, 79°N. *Mar. Geol.* **2017**, *390*, 282–300. [CrossRef]
12. Sun, Q.; Wu, S.; Hovland, M.; Luo, P.; Lu, Y.; Qu, T. The Morphologies and Genesis of Mega-Pockmarks near the Xisha Uplift, South China Sea. *Mar. Pet. Geol.* **2011**, *28*, 1146–1156. [CrossRef]
13. Tchesunov, A.; Ingels, J.; Popova, E. Marine Free-Living Nematodes Associated with Symbiotic Bacteria in Deep-Sea Canyons of North-East Atlantic Ocean. *J. Mar. Biol. Assoc. United Kingd.* **2012**, *92*, 1257–1271. [CrossRef]
14. Schroot, B.M.; Schüttenhelm, R.T. Shallow Gas and Gas Seepage: Expressions on Seismic and Other acoustic Data from the Netherlands North Sea. *J. Geochem. Explor.* **2003**, *78*, 305–309.
15. Jedari-Eyvazi, F.; Bayrakci, G.; Minshull, T.; Bull, J.; Henstock, T.; Macdonald, C.; Robinson, A. Seismic Characterization of a Fluid Escape Structure in the North Sea: The Scanner Pockmark Complex Area. *Geophys. J. Int.* **2023**, *234*, 597–619. [CrossRef]
16. Hovland, M.; Svensen, H. Submarine Pingoes: Indicators of Shallow Gas Hydrates in a Pockmark at Nyegga, Norwegian Sea. *Mar. Geol.* **2006**, *228*, 15–23. [CrossRef]
17. Vaular, E.; Barth, T.; Haflidason, H. The Geochemical Characteristics of the Hydrate-Bound Gases from the Nyegga Pockmark Field, Norwegian Sea. *Org. Geochem.* **2010**, *41*, 437–444. [CrossRef]
18. Kumar, A.; Cook, A.; Lawal, M.; Portnov, A.; Lecours, V. Pockmark Occurrence in the Northern Gulf of Mexico Influenced by Glacial Cycles and Hydrate Stability. *Geochem. Geophys. Geosystems* **2025**, *26*, e2024GC011781. [CrossRef]
19. Argnani, A.; Rovere, M. Submarine Morphology Offshore Crotone (Calabrian Accretionary Prism, Central Mediterranean): Pockmark Fields and Mud Extrusion in a Mobile Shale Domain. *Mar. Pet. Geol.* **2025**, *181*, 107530. [CrossRef]
20. Dimitrov, L.; Woodside, J. Deep Sea Pockmark Environments in the Eastern Mediterranean. *Mar. Geol.* **2003**, *195*, 263–276. [CrossRef]
21. Roelofse, C.; Alves, T.; Gafeira, J. Structural Controls on Shallow Fluid Flow and Associated Pockmark Fields in the East Breaks Area, Northern Gulf of Mexico. *Mar. Pet. Geol.* **2020**, *112*, 104074. [CrossRef]
22. Zhu, S.; Li, X.; Zhang, H.; Sha, Z.; Sun, Z. Types, Characteristics, Distribution, and Genesis of Pockmarks in the South China Sea: Insights from High-Resolution Multibeam Bathymetric and Multichannel Seismic Data. *Int. Geol. Rev.* **2021**, *63*, 1682–1702.
23. Li, X.; Guo, X.; Tian, F.; Fang, X. The Effects of Controlling Gas Escape and Bottom Current Activity on the Evolution of Pockmarks in the Northwest of the Xisha Uplift, South China Sea. *J. Mar. Sci. Eng.* **2024**, *12*, 1505. [CrossRef]
24. Yu, K.; Li, W.; Xu, J.; Zhan, W.; Yang, Y.; Miramontes, E. Interaction of Turbidity Currents Traversing a Pockmark Field: Insights for Submarine Channel Inception. *J. Geophys. Res. Earth Surf.* **2025**, *130*, e2025JF008394. [CrossRef]
25. Yu, K.; Miramontes, E.; Alves, T.; Li, W.; Liang, L.; Li, S.; Zhan, W.; Wu, S. Incision of Submarine Channels Over Pockmark Trains in the South China Sea. *Geophys. Res. Lett.* **2021**, *48*, e2021GL092861. [CrossRef]
26. Wang, X.; Zhao, M.; He, X.; Zhang, J.; Cheng, J.; Mao, H. Seismic Imaging Revealing the Processes from Subduction to Arc-Continental Collision in the Northeastern South China Sea. *Tectonophysics* **2025**, *902*, 230684. [CrossRef]
27. Zhang, C.; Manatschal, G.; Taylor, B.; Sun, Z.; Zhao, M.; Zhang, J. Characterization and Mapping of Continental Breakup and Seafloor Spreading Initiation: The Example of the Northern Rifted Margin of the South China Sea. *Basin Res.* **2024**, *36*, e12882. [CrossRef]
28. Wu, Z.; Zhang, J.; Xu, M.; Li, H. Magnetic Anomaly Lineations in the Northeastern South China Sea and Their Implications for Initial Seafloor Spreading. *Front. Earth Sci.* **2023**, *10*, 1015856. [CrossRef]
29. Briais, A.; Patriat, P.; Tapponnier, P. Updated Interpretation of Magnetic-Anomalies and Sea-Floor Spreading Stages in the South China Sea—Implications for the Tertiary Tectonics of Southeast-Asia. *J. Geophys. Res. Solid Earth* **1993**, *98*, 6299–6328. [CrossRef]
30. Lei, C.; Alves, T.; Ren, J.; Tong, C. Rift Structure and Sediment Infill of Hyperextended Continental Crust: Insights From 3D Seismic and Well Data (Xisha Trough, South China Sea). *J. Geophys. Res.-Solid Earth* **2020**, *125*, e2019JB018610. [CrossRef]
31. Ma, R.; Liu, C.; Li, Q.; Jin, X. Calcareous Nannofossil Changes in Response to the Spreading of the South China Sea Basin during Eocene-Oligocene. *J. Asian Earth Sci.* **2019**, *184*, 103963. [CrossRef]
32. Deng, P.; Mei, L.; Liu, J.; Zheng, J.; Liu, M.; Cheng, Z.; Guo, F. Episodic Normal Faulting and Magmatism during the Syn-Spreading Stage of the Baiyun Sag in Pearl River Mouth Basin: Response to the Multi-Phase Seafloor Spreading of the South China Sea. *Mar. Geophys. Res.* **2019**, *40*, 33–50.
33. Ma, P.; Liu, Z.; Huang, B.; Zhao, Y.; Shu, W.; Li, Y. Oligocene Evolution of the Outermost Continental Margin in Response to Breakup and Early Spreading of the South China Sea. *Mar. Geol.* **2020**, *427*, 106241. [CrossRef]
34. Chen, W.; Yan, Y.; Carter, A.; Clift, P.; Huang, C.; Yumul, G.J.; Dimalanta, C.; Gabo-Ratio, J.; Zhang, L.; Wang, M.; et al. Evolution of Arc-Continent Collision in the Southeastern Margin of the South China Sea: Insight From the Isugod Basin in Central-Southern Palawan. *Tectonics* **2024**, *43*, 8078. [CrossRef]

35. Yin, S.; Li, J.; Ding, W.; Sawyer, D.; Wu, Z.; Tang, Y. Sedimentary Filling Characteristics of the South China Sea Oceanic Basin, with Links to Tectonic Activity during and after Seafloor Spreading. *Int. Geol. Rev.* **2020**, *62*, 887–907.
36. Schluter, H.; Hinz, K.; Block, M. Tectono-Stratigraphic Terranes and Detachment Faulting of the South China Sea and Sulu Sea. *Mar. Geol.* **1996**, *130*, 39. [CrossRef]
37. Zhu, W.; Xie, X.; Wang, Z.; Zhang, D.; Zhang, C.; Cao, L.; Shao, L. New Understanding of the Origin of the Xisha Uplift Basement in the South China Sea. *Sci. Sin. (Terrae)* **2017**, *47*, 1460–1468.
38. Gao, J.; Bangs, N.; Wu, S.; Cai, G.; Han, S.; Ma, B.; Wang, J.; Xie, Y.; Huang, W.; Dong, D. Post-seafloor Spreading Magmatism and Associated Magmatic Hydrothermal Systems in the Xisha Uplift Region, Northwestern South China Sea. *Basin Res.* **2019**, *31*, 688–708. [CrossRef]
39. Yang, Z.; Zhang, G.; Fan, G.; Lu, Y.; Shao, D.; Liu, S.; Wang, W. Tectonic Subsidence and Its Response to Geological Evolution in the Xisha Area, South China Sea. *Appl. Sci.* **2023**, *13*, 13127268. [CrossRef]
40. Wu, S.; Yang, Z.; Wang, D.; Lu, F.; Lüdmann, T.; Fulthorpe, C.; Wang, B. Architecture, Development and Geological Control of the Xisha Carbonate Platforms, Northwestern South China Sea. *Mar. Geol.* **2014**, *350*, 71–83. [CrossRef]
41. Xie, X.; Müller, R.D.; Ren, J.; Jiang, T.; Zhang, C. Stratigraphic Architecture and Evolution of the Continental Slope System in Offshore Hainan, Northern South China Sea. *Mar. Geol.* **2008**, *247*, 129–144. [CrossRef]
42. Shao, L.; Cui, Y.; Qiao, P.; Zhang, D.; Liu, X.; Zhang, C. Sea-Level Changes and Carbonate Platform Evolution of the Xisha Islands (South China Sea) since the Early Miocene. *Palaeogeogr. Palaeoclimatol. Palaeoecol.* **2017**, *485*, 504–516. [CrossRef]

Disclaimer/Publisher's Note: The statements, opinions and data contained in all publications are solely those of the individual author(s) and contributor(s) and not of MDPI and/or the editor(s). MDPI and/or the editor(s) disclaim responsibility for any injury to people or property resulting from any ideas, methods, instructions or products referred to in the content.